Composites Part B 234 (2022) 109667

Contents lists available at ScienceDirect

Composites Part B

journal homepage: www.elsevier.com/locate/compositesb

A strategy of functional crosslinking acellular matrix in blood-contacting implantable devices with recombinant humanized collagen type III (rhCOLIII)

Yao Ge [a], Gaoyang Guo [a], Kunpeng Liu [a], Fan Yang [a], Li Yang [a,**], Yunbing Wang [a,*], Xingdong Zhang [a]

[a] National Engineering Research Center for Biomaterials, Sichuan University, Chengdu, 610064, PR China

ARTICLE INFO

Keywords:
Blood-contacting implantable device
Heart valve
Recombinant humanized collagen
Functional crosslinking method
Anticoagulation
Mechanical property

ABSTRACT

A large number of blood contacting implantable devices are used worldwide annually. Acellular matrix (AM), as one of the blood-contacting materials, has achieved a great success, since it remains the structures, components and certain functions of extracellular matrix. However, AM often fails during the period of service owing to non-ideal anticoagulation, severe inflammatory responses and poor mechanical properties. Herein, we specially prepared a newly designed tailored recombinant humanized collagen type III (rhCOLIII) that effectively removed the binding site to platelets while retaining cytocompatibility. In this study, a radical-polymerization-crosslinked decellularized porcine pericardium (DPP) with rhCOLIII and glycidyl methacrylate (GMA) through one-pot method was designed as artificial heart valves. Due to the introduction of rhCOLIII, the anticoagulation properties were dramatically improved with fewer platelets adhesion and less thrombogenesis. The mechanical properties of the novel heart valve (rhCOLIII/GMA-DPP) were significantly enhanced through radical polymerization crosslinking. Furthermore, experiments in vivo and vitro showed the inflammatory responses were moderately reduced. In conclusion, this study provides a simple strategy for functional crosslinking AM in blood-contacting implantable devices and shows possibilities for real application.

1. Introduction

Acellular matrix (AM) is a promising natural biomaterial for manufacturing blood-contacting implantable devices as it preserves the three-dimensional structures, compositions and certain functions of extracellular matrix compared with synthetic materials [1–5]. However, AM often fails during the period of service owing to the existence of defects in thrombogenesis, severe inflammatory responses and rapid degradability [6–8].

The anticoagulation properties of blood-contacting implantable materials are the most important during the interaction with blood [9–12]. The thrombogenic nature can induce severe complications for patients, and eventually functional failure [13]. Therefore, it is indispensable to reduce or avoid thrombosis caused by platelet activation, contact coagulation factors and tissue factor [14]. The common method to solve above issue is decellularization before being implanted [15,16]. Nevertheless, during the decellularization, tertiary structure of AM constituents may be impaired and structures of highly thrombogenic collagen are exposed, which might lead to adhering and activating platelets as well as coagulation factor XII [17,18]. Generally, two main methods of surface modification are adopted. The first is to design a non-adhesive, inert, non-biofouling surface, and the second aims to bio-functionalize the surface which can activate a cascade of biological events [19–22]. But current methods are limited and cannot match anticoagulant abilities of native blood vessels [23,24]. Apart from thrombogenesis, proteins in blood and interstitial fluids will immediately adhere to biomaterials surface after first contacting with tissues of recipients, leading to inflammatory responses. Severe inflammatory responses can lead to biomaterials failure and sometimes life-threatening. In addition, they can activate and destroy the blood components and elements of the inflammatory system also participate in thrombogenesis [25,26]. Despite decellularization, cell debris and genetic materials cannot be taken out completely. Therefore, xenoantigenicity of AM may induce a degree of immune response [27]. Moreover, AM is prone to

* Corresponding author.
** Corresponding author.
E-mail addresses: yanglisc@scu.edu.cn (L. Yang), yunbing.wang@scu.edu.cn (Y. Wang).

https://doi.org/10.1016/j.compositesb.2022.109667
Received 10 November 2021; Received in revised form 29 December 2021; Accepted 18 January 2022
Available online 29 January 2022

rapid degradation, resulting in failure in tissues' or organs' repair and device failure. Hence, a suitable method is needed to improve those defects [18].

Recombinant humanized collagen has attracted wide attention due to its high bioactivity, designability, low immunogenicity, good water solubility and no virus risk [28,29]. Despite their advantages, the application in blood-contacting modification has rarely been reported. And it is known that in complete amino acid sequence of collagen, hydroxyproline (O)-containing sequences, such as GLOGEN, GROGER, GLOGER, GFOGER, can readily bind to platelets' surface integrin GP Ia/IIa (α2β1), GP VI and GP Ib/IX/V complexes, thereby activating platelets and inducing coagulation [30]. Hence, in order to gain anticoagulation properties, we designed a newly designed tailored recombinant humanized collagen type III (rhCOLIII) without O in our previous report, which originated from active peptide sequences of human type III collagen Gly483-Pro512. Meanwhile, the highly adhesive fragments including Gly-Glu-Lys (GEK) and Gly-Glu-Arg (GER) triplets retained in it makes contributions to cytocompatibility [31,32]. Additionally, our previous reports have developed a simply radical polymerization crosslinking method for AM, which has good biocompatibility and the potential to functionalize tissues expediently [33,34].

In this study, rhCOLIII is prepared and modified to AM (decellularized porcine pericardium, DPP), with glycidyl methacrylate (GMA), through radical-polymerization-crosslinking and one-pot methods [35,36]. It is hoped that the modified DPP can possess anticoagulation properties and good biocompatibility while enhancing its stability. The chemical structures, DPP stability, mechanical properties, anticoagulation properties, immune responses, cytotoxicity, and calcification are further examined in vivo or in vitro. The aim of the research is to provide a simple strategy for functional crosslinking AM and possibilities for real application in blood-contacting implantable devices.

2. Materials and methods

2.1. Materials

Fresh porcine pericardium (FPP) was offered by Venus Medical Appliances Co., Ltd. (Hangzhou, China). rhCOLIII with special structure was designed by us and prepared by Jingbo Co., Ltd. (Shanxi, China). GMA was purchased from Adamas. Sodium bisulfite and ammonium persulfate were purchased from Greagent. Glutaraldehyde (glu) was purchased from Adamas. RNase and DNase were purchased from Macklin. Cell-counting kit-8 (cck-8) was purchased from Dojindo (Kumamoto, Japan). Raw264.7 cells and mouse fibroblasts L929 were gained from Cell-bank of Chinese Academy of Sciences. Lactate dehydrogenase (LDH) assay kit was bought from Beyotime Biotechnology Co., Ltd. (Shanghai, China). Rat IL-10, TNF-α ELISA Kits were purchased from mlbio Co., Ltd. (Shanghai, China). Calcein acetoxymethyl ester (calcein AM) was bought from Sigma-Aldrich.

2.2. Decellularization

FPP was decellularized as our previous study. In short, the first detergent step was to immerse FPP in a mixture solution with 0.5% (w/v) sodium deoxycholate, 0.5% (w/v) TrionX-100, 0.02% (w/v) ethylenediaminetetraacetic acid disodium salt for 48 h. Then, the resulting FPP was incubated in Tris-buffer (10 mmol/L Tris-HCl, 2.5 mmol/L magnesium chloride, 0.5 mmol/L calcium chloride, pH = 7.6), adding 150 U/ml DNase and 15 μg/ml RNase for another 48 h in digestion step. Ultimately, FPP was rinsed with deionized water completely and stored in glycerin at −20 °C.

To measure the decellularization degree, FPP and DPP were fixed in 10% formaldehyde, then dehydrated with ethanol and xylene, embedded in paraffin. Then slices stained with hematoxylin and eosin (H&E) were used to visualize cells and slices stained with Masson's trichrome (MT) were used to analyze collagen. Regarding further analysis of DNA quantification, tissue pieces were weighed after freeze drying. Then DNeasy Blood & tissue kit (Qiagen, Beijing, China) and picogreen Kit (Yeasen Biotech, Shanghai, China) were applied to extract and quantify DNA of FPP and DPP respectively. All operations were in accordance with the supplier's instructions.

2.3. Crosslink DPP

Glutaraldehyde crosslinking DPP (GLU-DPP): DPP was cross-linked with 0.625% (w/v) glu solutions at room temperature for 7 days under gentle shaking. Then the GLU-DPP was stored in 0.2% (v/v) glu solutions.

GMA crosslinking DPP (GMA-DPP): Briefly, DPP was washed with deionized water entirely to remove glycerin and then was immersed in four different solutions for 7 days at 37 °C, PBS with varying concentrations of GMA (0.5%, 1%, 3%, 5%, v/v). Subsequently, redox-initiator 50 mM sodium bisulfite (SBS) and 50 mM ammonium persulfate (APS) were added to the mixture solution to initiate a cross-linking reaction at 37 °C for 6 h.

rhCOLIII/GMA-DPP: The preparation was mainly through "one-pot" method and radical crosslinking (Fig. 1). In brief, DPP was immersed in a mixture solution with 1 mg/ml rhCOLIII and 5% (w/v) GMA in PBS at 37 °C for 7 days. The resulting DPP was then cross-linked by the 50 mmol/L SBS and 50 mmol/L APS for 6 h at 37 °C.

2.4. Physicochemical characterization

2.4.1. Enzymatic degradation

DPP and cross-linked DPPs were cut into approximately 1 × 1 cm^2 small pieces and weighed (W_0). Then they were incubated in 1 mL Tris-buffer (0.1 mol/L Tris-HCl, 1 mmol/L calcium chloride, pH = 7.6), adding collagenase II (125 U/ml) at 37 °C for 12 h. After degradation, processed tissues were rinsed, freeze-dried, weighed again (W_1). The degree of lost weight was measured as below formula:

$$\mathrm{Degree\cdot of\cdot lost\cdot weight}\frac{W_0 - W_1}{W_0} \times 100\%$$

2.4.2. Amine content measurement

Free amine content of tissues was generally quantified through a ninhydrin assay. In brief, ninhydrin work solution (NWS) was prepared as previously described. DPP and DPP after treating with the mixture solution containing GMA and rhCOLIII for 7 days (7d-DPP) were weighed after cutting into small pieces and then immersed in 1 ml NWS at 100 °C for 20 min. To test the change of amino contents of rhCOLIII solutions before and after the 7 days' reaction, 400 μl 1 mg/ml rhCOLIII solution and 400ul 7 days' mixture solution (7d-rhCOLIII) were collected and then reacted with 1 ml NWS at 100 °C for 20 min. After cooling down to 25 °C, 200 μl 50% (w/v) isopropanol was added to terminate reaction. Supernatants' absorbance at 570 nm was assayed by microplate reader (Bio-Tek). The amine content was decided with formulae below:

$$\mathrm{Amino\cdot content\cdot} = \cdot\frac{\boldsymbol{OD}_{sample}}{\boldsymbol{weight}_{sample}}\cdot\mathrm{Amino\cdot content\cdot} = \cdot\frac{\boldsymbol{OD}_{sample}}{\boldsymbol{volume}_{sample}}$$

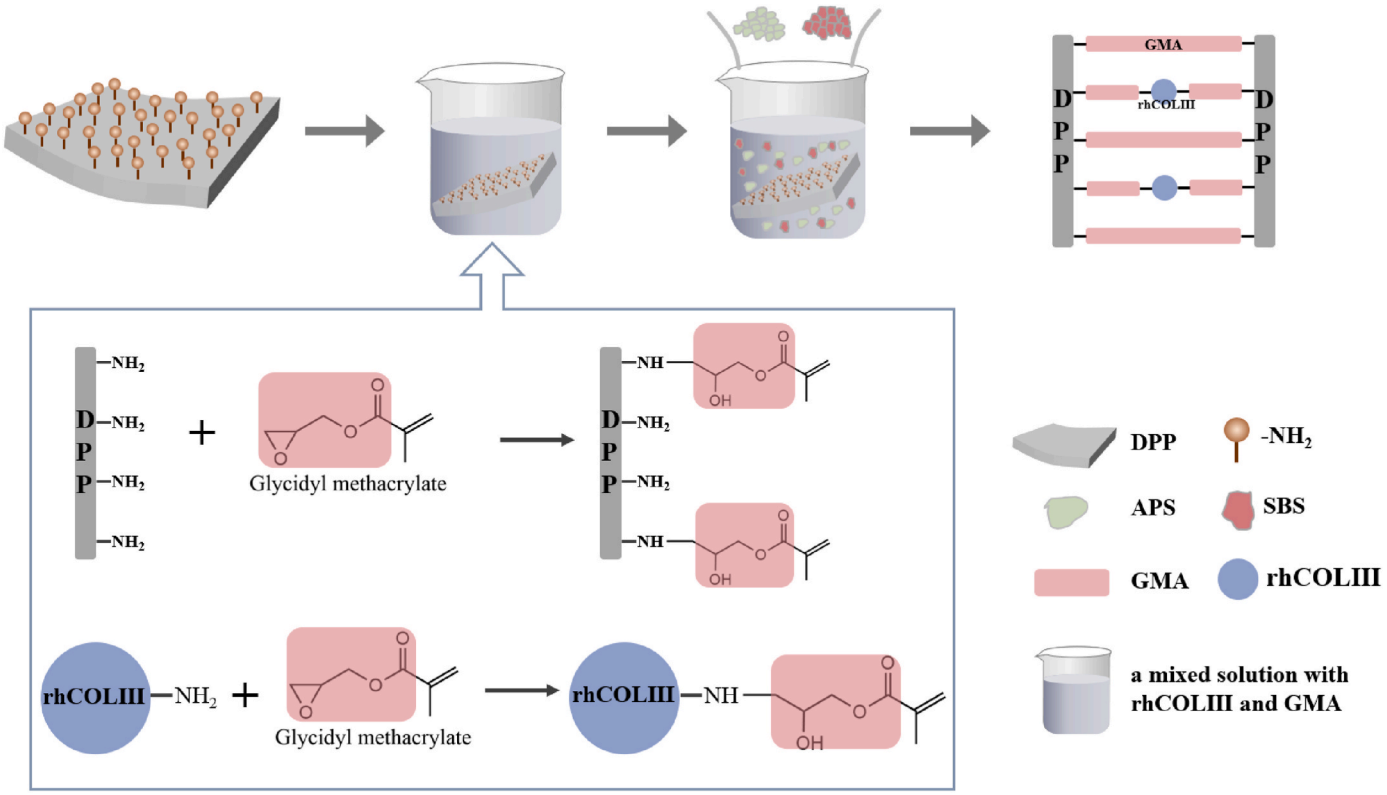

Fig. 1. Schematic diagram of rhCOLIII/GMA-DPP scaffolds preparation.

2.4.3. Attenuated total reflectance fourier transform infrared (ATR-FTIR) spectroscopy

Materials were cut into small pieces after freeze-drying. ATR-FTIR (West Palm Beach, FL) with wavelength ranging from 800 to 4000 cm^{-1} was used to verify the chemical and structural properties and rhCOLIII/GMA-DPP, GMA-DPP, DPP.

2.4.4. ^1H NMR spectroscopy

The tissues were cut into small pieces and were dissolved by deuterium chloride for 24 h at 37 °C. The hydrolysates were centrifuged at 4000 rpm to remove residual tissues and the supernatants were collected. ^1H NMR analysis was obtained by a Bruker Avance 400 MHz spectrometer.

2.4.5. Fluorescent visualization of rhCOLIII on DPP

To confirm the success of rhCOLIII modifying DPP, FITC-labeled rhCOLIII (FITC-rhCOLIII) was used to prepared rhCOLIII/GMA-DPP in the same way. For FITC-rhCOLIII, rhCOLIII and FITC were mixed at the ratio of 4:1 (weight) in saturated Na_2CO_3 solutions were magnetically stirred at 25 °C for 12 h. After dialysis against distilled water with cellulose tube (MWCO 1000 Da) under dark conditions for 2 days, the mixture solution was lyophilized and stored as FITC-rhCOLIII sponges. For crosslinking DPP, the method was as described in 2.3 except that rhCOLIII was replaced by FITC-rhCOLIII. A fluorescence microscope (Leica DMI 4000, Germany) was applied to obtain fluorescence images of tissues cross sections and surfaces.

2.4.6. Tensile test

Mechanical properties of rhCOLIII/GMA-DPP, GMA-DPP, GLU-DPP and DPP were tested with a tensile tester (Cellscale, CA). Tissue materials were prepared in rectangle strips (25 mm × 5 mm). Three random thicknesses of each sample were scaled with the thickness gauge. When

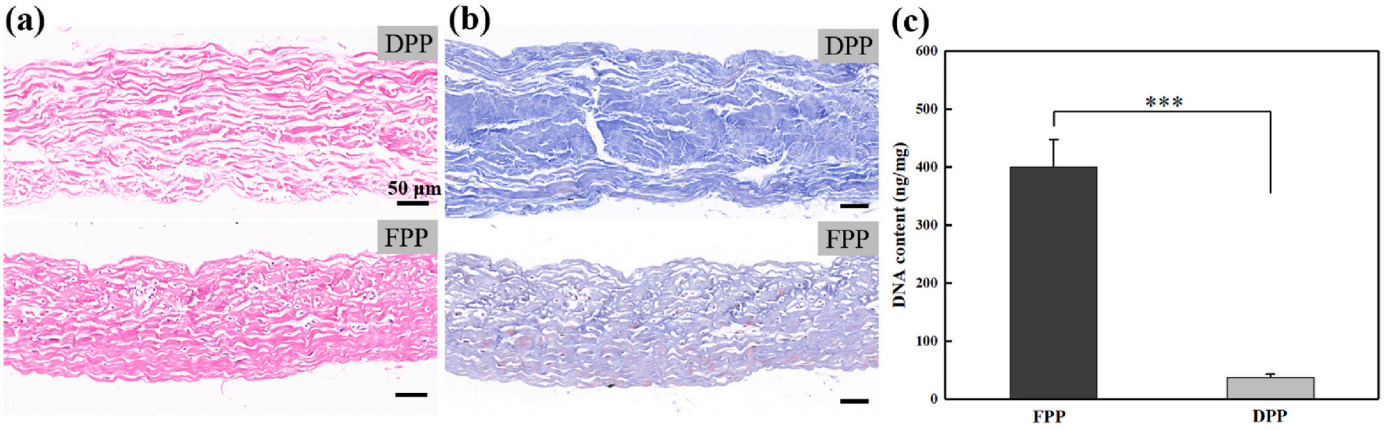

Fig. 2. Decellularization degree. (a) H&E staining on sections of FPP and DPP. (b) MT staining on sections of FPP and DPP. (c) DNA quantification of FPP and DPP.

testing, samples were stretched under PBS soaking condition, using a constant speed until failure, 18 mm/min. Elongation and tensile strength were calculated as previously described.

2.5. Evaluation of hemocompatibility

2.5.1. Platelet adhesion

To assay a degree of adhering platelet, whole blood was obtained from Laboratory Animal Center at Sichuan University legally. Before testing, whole blood was centrifuged for about 15 min at1500 rpm to obtain platelet-rich plasma (PRP). rhCOLIII/GMA-DPP, GMA-DPP, GLU-DPP and DPP materials were cut to a 96-well plate size and rinsed for 3 times with PBS. Then they were incubated with 100 μl PRP for 1 h at 37 °C and washed with PBS 3 times again. To visualize the platelets adhesion on samples, 40 μM calcein AM solutions were used to stain samples for 30min before observed by fluorescence microscope. To observe platelets' morphology, samples were fixed in 2.5% glu and then dehydrated by ethanol (30%, 50%, 80%, 100%). Morphology images were acquired through scanning electron microscope (SEM). To quantification the adherent platelets, the LDH assay was performed and all procedures were in accordance with the supplier's instructions.

2.5.2. Recalcification the whole blood clotting assay

This assay was performed as our previous studies. In brief, all materials were rinsed for 3 times with PBS, and then immersed in fresh whole blood with 100 mM 3% (v/v) calcium chloride solutions at 37 °C for 10–15 min. After rinsing with PBS, samples were soaked in 350 μl 0.5% (w/v) TrionX-100 solutions to dissolve thrombi until no residual thrombus was observed. The OD of supernatant at 405 nm was tested.

2.5.3. In vitro antithrombogenicity

All experiments on animals were allowed by Medical Ethics Committee at Sichuan University. New Zealand white rabbits (n = 3) weighted 3–3.5 kg were chosen and injected pentobarbital sodium. Right external jugular vein and left carotid artery were peeled and jointed by a polyvinyl chloride (PVC) catheter with 4 kinds of samples (1.5 cm × 1 cm) rolling in. Before testing, the PVC catheter was washed with normal saline (NS). After extracorporeal circulation for 40 min, materials were taken out, washed with NS, photographed, fixed with 2.5% (v/v) glu and observed by SEM.

2.6. Cytotoxicity

The cytotoxicity assay was finished as ISO 10993–5:2009 described. In brief, conditioned mediums were prepared through immersing rhCOLIII/GMA-DPP, GMA-DPP, GLU-DPP and DPP samples in Dulbecco's modified Eagle's essential medium at 0.2 g/ml for 72 h respectively. Before preparation, tissues were sterilized with ozone (O_3). L929 fibroblasts were cultured in a 96-well plate (10,000 cells/well) for 4 h to guarantee cells to adhere to the wall. The culture was then continued for 1 day and 3 days in a 5-times diluted conditioned medium. Cell viability was evaluated by a CCK-8 assay kit.

2.7. Quantitation of inflammatory potential and immunofluorescence staining

After aseptic processing, macrophages RAW 264.7 were seeded on the material surfaces in a 96-well plate (20,000 cells/well). After cultured for 1 day, the supernatant of medium was centrifuged to measure the release of inflammatory factor IL-6 and TNF-α by ELISA kits. All operations were in accordance with the supplier's instructions. Regarding immunofluorescence staining, cells were washed with PBS and fixed with 4% paraformaldehyde for 20 min. After that, cells were interacted with mouse *anti*-TNF-α (1:200 dilution) and *anti*-IL-6 antibodies (1:200 dilution) overnight at 4 °C. Finally, macrophages were treated with FITC-labeled secondary antibody for 1–2 h and DAPI for 5

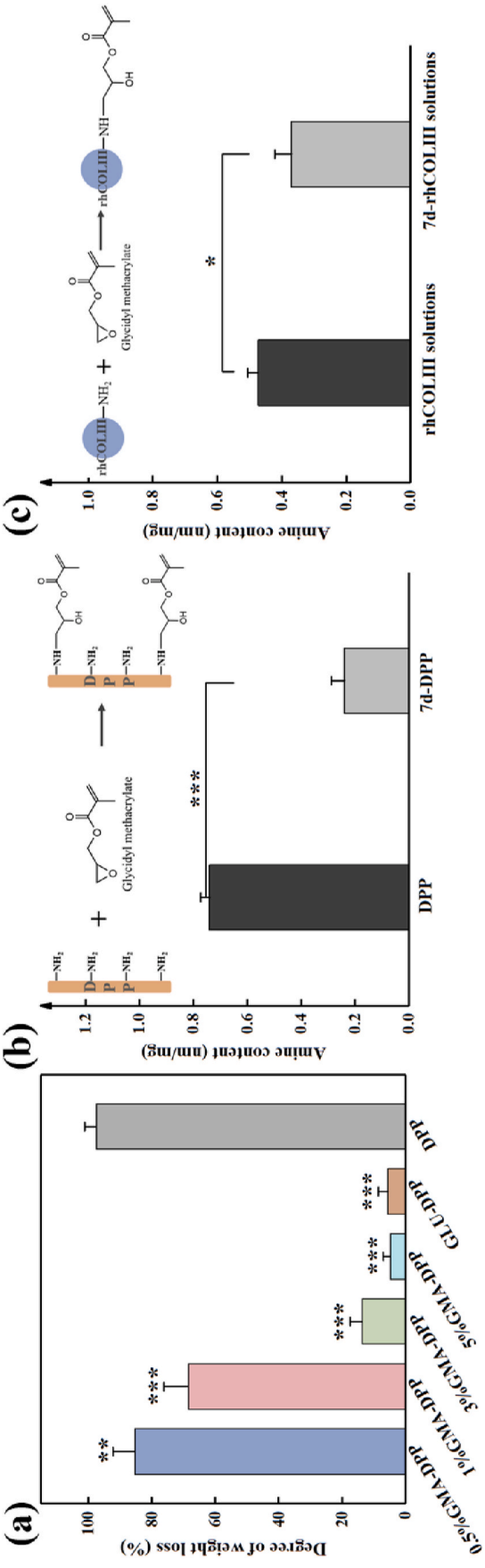

Fig. 3. (a) Resistance to enzymatic degradation for 6 types of issues. Lost weight degree of 0.5%GMA-DPP, 1%GMA-DPP, 3% GMA-DPP, 5% GMA-DPP, GLU-DPP, DPP after collagenase treatment. (* represents the significant difference with DPP). (b) Verification of reactive group amine content of DPP and 7d-DPP. (c) Amine content of rhCOLIII solutions and 7d-rhCOLIII solutions.

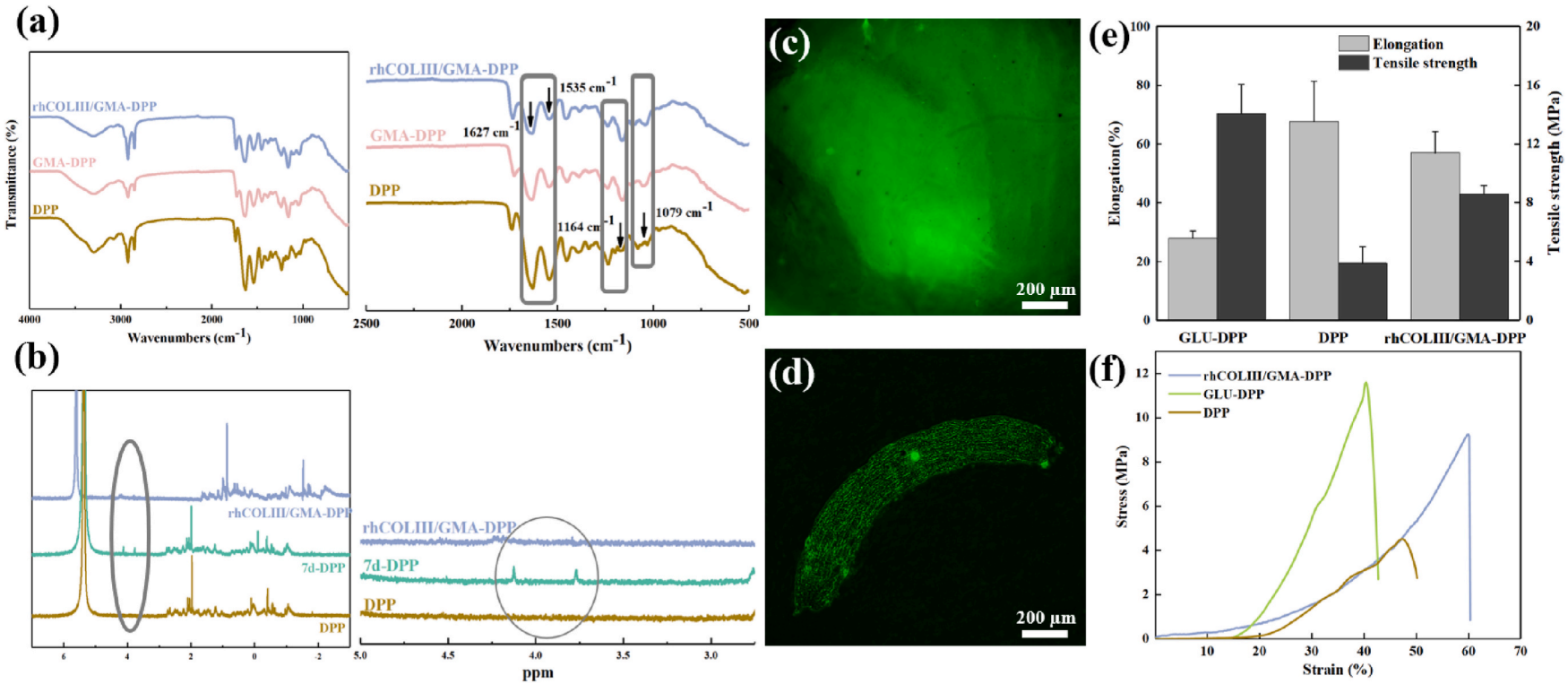

Fig. 4. Physical and chemical properties. (a) Representative ATR-FTIR spectrum of DPP, GMA-DPP and rhCOLIII/GMA-DPP. (b) Representative ^{1}H NMR spectrum of DPP, 7d-DPP and rhCOLIII/GMA-DPP. (c) Surface fluorescence image of FITC-labeled rhCOLIII/GMA-DPP. (d) Cross-section fluorescence image of FITC-labeled rhCOLIII/GMA-DPP. (e) Quantitative data for Tensile strength and Elongation. (f) Representative stress-strain curves.

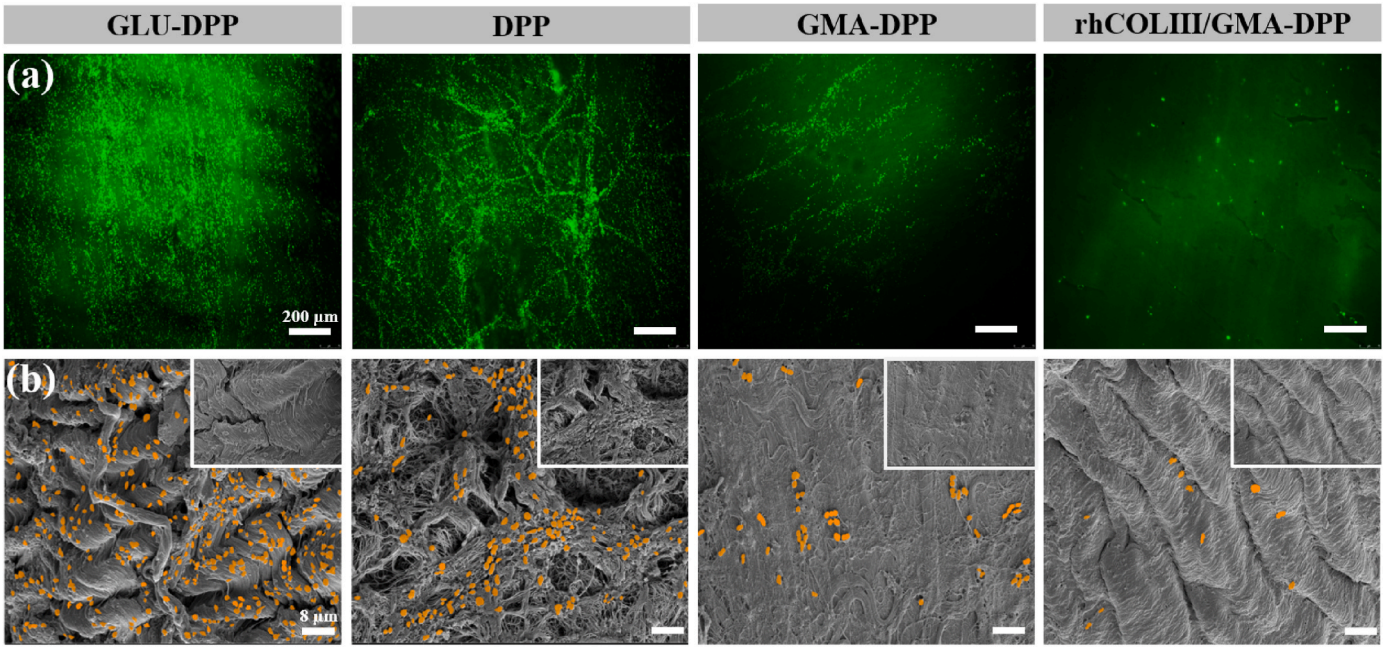

Fig. 5. Hemocompatibility. (a) Fluorescence images of platelets adhered on GLU-DPP, DPP, GMA-DPP and rhCOLIII/GMA-DPP surfaces. (b) SEM images of platelets morphology adhered on GLU-DPP, DPP, GMA-DPP and rhCOLIII/GMA-DPP surfaces.

min, respectively. All fluorescent images were obtained by CLSM.

2.8. Subcutaneous implantation and characterization

2.8.1. Subcutaneous implantation in rats

All kinds of tissues (rhCOLIII/GMA-DPP, GMA-DPP, GLU-DPP, DPP) were shaped into 1 cm × 1 cm strips and disinfected with O_3. Male Sprague-Dawley (SD) rats about 70–80 g were chosen and anesthetized with a 4% (w/v) chloral hydrate solution (8 ml/kg) through intraperitoneal injection (n = 6 in each group) beforehand. A surgical incision was made at both sides of the back of the SD rats. Tissues of each group were implanted subcutaneously as Fig. 9 shows. After implantation for 7, 14, 28 days, tissues surrounded by new fiber capsules were removed respectively and fixed with 4% paraformaldehyde.

2.8.2. Histological analysis

All fixed explant were dehydrated by ethanol solutions and xylene and cut into about 6 μm slices after embedding in paraffin. In histological analysis, sections stained with H&E were used to check biocompatibility of tissues in vivo. Antibody called anti-rat IL-6 and TNF-α were used to assess inflammation of 4 types of tissues in vivo. Sections stained with alizarin red was applied to examine the calcification of subcutaneous implantation in rats. All sections were observed by Slide scanner (Carl Zeiss Microimaging GmbH, Germany). The immunopositive cells were quantified by ImageJ software. Regarding immunohistochemical (IHC) staining, mouse anti-rat CD68 antibody was applied to label macrophages.

2.8.3. Quantitative analysis of calcium

To quantify an amount of calcium in tissues, explants were gently removed surrounding tissues, freeze-dried and weighted after implantation for 7, 14, 28 days. Then they were dissolved in 6 mol/L HCl for 6 h at 90 °C. ICP-OES (Agilent 720) was used to analyze the calcium content of samples.

2.9. Statistical analysis

All data was showed as mean ± standard deviation (SD), *$p < 0.05$, **$p < 0.01$, ***$p < 0.001$. One-way analysis of variance (ANOVA) was used to analyze differences between 2 groups and among more than 3 groups.

3. Results

3.1. Analysis of decellularization degree

Decellularized degree of FPP was analyzed by H&E, MT and DNA quantification test. H&E staining was used to analyze the removing degree of cellular components. Compared with FPP (Fig. 2a), few cellular components were detected. MT staining was used to measure collagen status and images showed slight disorders of collagen fibers in DPP (Fig. 2b). To further evaluate decellularization degree, DNA quantification was applied. Compared with FPP (400.0 ± 47.5 ng/mg), the total DNA content of DPP (38.0 ± 5.4 ng/mg) decreased significantly after decellularization. The results suggested that decellularization was effective to remove cellular components.

3.2. Collagen stability

Collagen stability test was applied to evaluate resistance of tissues against enzymatic degradation and select an optimal concentration for the following experiments. After collagenase treatment, the weight loss

of different ratios GMA-DPPs was shown in Fig. 3a. The weight loss ratio of 0.5%GMA-DPP (85.4 ± 6.9%) and 1%GMA-DPP (68.5 ± 7.8%) was close to DPP (97.6 ± 3.7%), indicating a pretty low crosslinking degree to protect collagen. The weight loss ratio of 5%GMA-DPP (13.8 ± 3.8%) was the lowest and was close to GLU-DPP (14.8 ± 2.2%) which was the most common commercial bioprosthetic heart valves. The results demonstrated that 5%GMA-DPP was optimal for this study that could stabilize collagen and crosslink DPP effectively.

3.3. Physical and chemical characterization

Amine group of DPP and rhCOLIII was supposed to be a main reaction site with epoxy group of GMA. To verify this hypothesis, the free amine content of DPP and 7d-DPP were tested (Fig. 3b). Compared with DPP (0.74 ± 0.03 ng/mg), amine content of 7d-DPP (0.24 ± 0.05 ng/mg) decreased, indicating that amine group reacted with epoxy group effectively. Likewise, amine content of rhCOLIII solutions reduced from 0.47 ± 0.03 ng/mg to 0.37 ± 0.05 ng/mg after reacting with GMA (Fig. 3c). These outcomes confirmed the success of the conjugation of GMA to DPP and rhCOLIII.

ATR-FTIR and ^{1}H NMR were used to further characterize chemical and structural changes on surfaces of tissues. As shown in Fig. 4a, the N–H bending vibration occurred in the 1650 - 1590 cm^{-1} region and the peak intensity of GMA-DPP, rhCOLIII/GMA-DPP decreased compared with DPP due to the consumption of amine group. Since a large number of free amine groups on DPP surfaces, two peaks of C–N stretching vibration were observed in DPP at 1079 cm^{-1}. But no obvious two-peaks were observed in another two samples. GMA-DPP and rhCOLIII/GMA-DPP presented the signal of C–O–C stretching vibration at 1164 cm^{-1}, which was a part of GMA structure.

^{1}H NMR spectra was applied to characterize the conversion of vinyl groups on the surface of tissues. In Fig. 4b, the presence of vinyl groups (4.11 ppm and 3.75 ppm) represented the introduction of methacrylate groups. After radical polymerization, no vinyl groups signal was detected, demonstrating success in crosslinking DPP.

To visualize rhCOLIII modification, FITC-labeled rhCOLIII was used. Green fluorescence on FITC-labeled rhCOLIII of rhCOLIII/GMA-DPP was observed (Fig. 4c and d). It suggested that rhCOLIII was successfully introduced onto GMA-DPP.

3.4. Mechanical property

Tensile strength and elongation of DPP, GMA-DPP, rhCOLIII/GMA-DPP were tested to characterize mechanical properties. According to Fig. 4e and f, the tensile strength of rhCOLIII/GMA-DPP (8.6 ± 0.5 MPa) was prominently enhanced after functional crosslinking DPP (3.8 ± 1.1 MPa). Furthermore, elongation of DPP was the highest (67.8 ± 13.7%) and GLU was lowest (28.0 ± 2.5%). The elongation of rhCOLIII/GMA-DPP (57.1 ± 7.2%) was close to DPP.

3.5. Hemocompatibility analysis

Hemocompatibility was characterized by platelet adhesion test, recalcification whole blood clotting assay and ex vivo arteriovenous shunt assay. According to Fig. 5a, green fluorescent spots represented platelets. A large amount of green fluorescent spots was found on GLU-DPP and DPP. The number of platelets adhered to GMA-DPP decreased significantly. After the introduction of rhCOLIII, minimal platelet adhesion was observed on rhCOLIII/GMA-DPP. Likewise, the results of SEM images were consistent with the fluorescence images, as shown in Fig. 5b. Irregular platelet spreading and pseudopodia characteristics were displayed on GLU-DPP and DPP, which were the signs of activated platelets. In addition, platelets were quantified by LDH release assay and the number of adhered platelets was the lowest in rhCOLIII/GMA-DPP group (Fig. 6c).

The whole blood clotting assay in vitro was performed to test antithrombogenic properties. Thrombogenesis images of GLU-DPP,

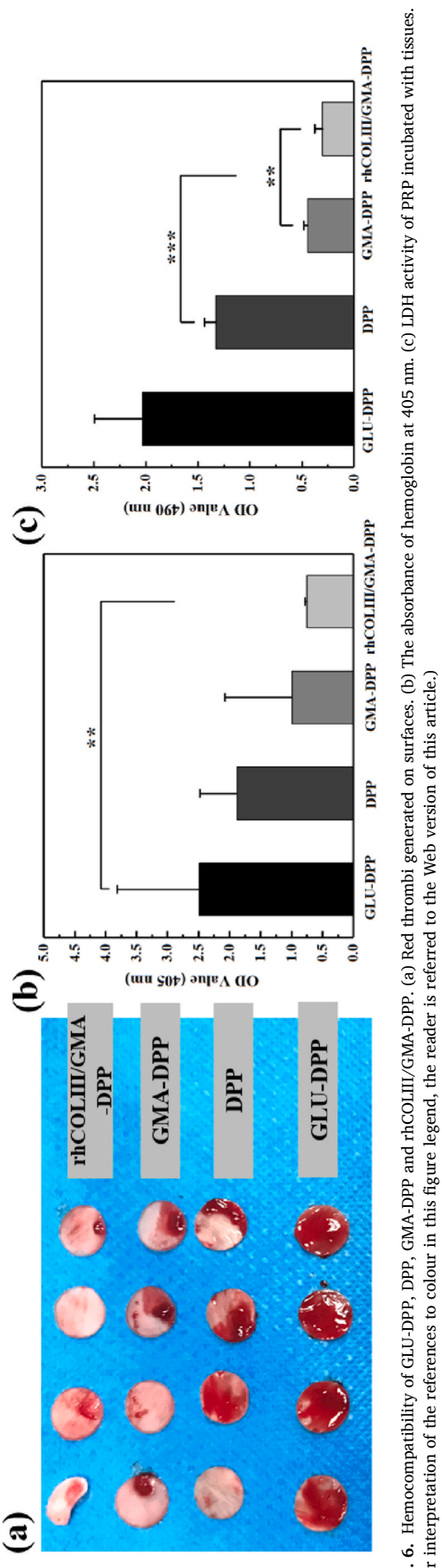

Fig. 6. Hemocompatibility of GLU-DPP, DPP, GMA-DPP and rhCOLIII/GMA-DPP. (a) Red thrombi generated on surfaces. (b) The absorbance of hemoglobin at 405 nm. (c) LDH activity of PRP incubated with tissues. (For interpretation of the references to colour in this figure legend, the reader is referred to the Web version of this article.)

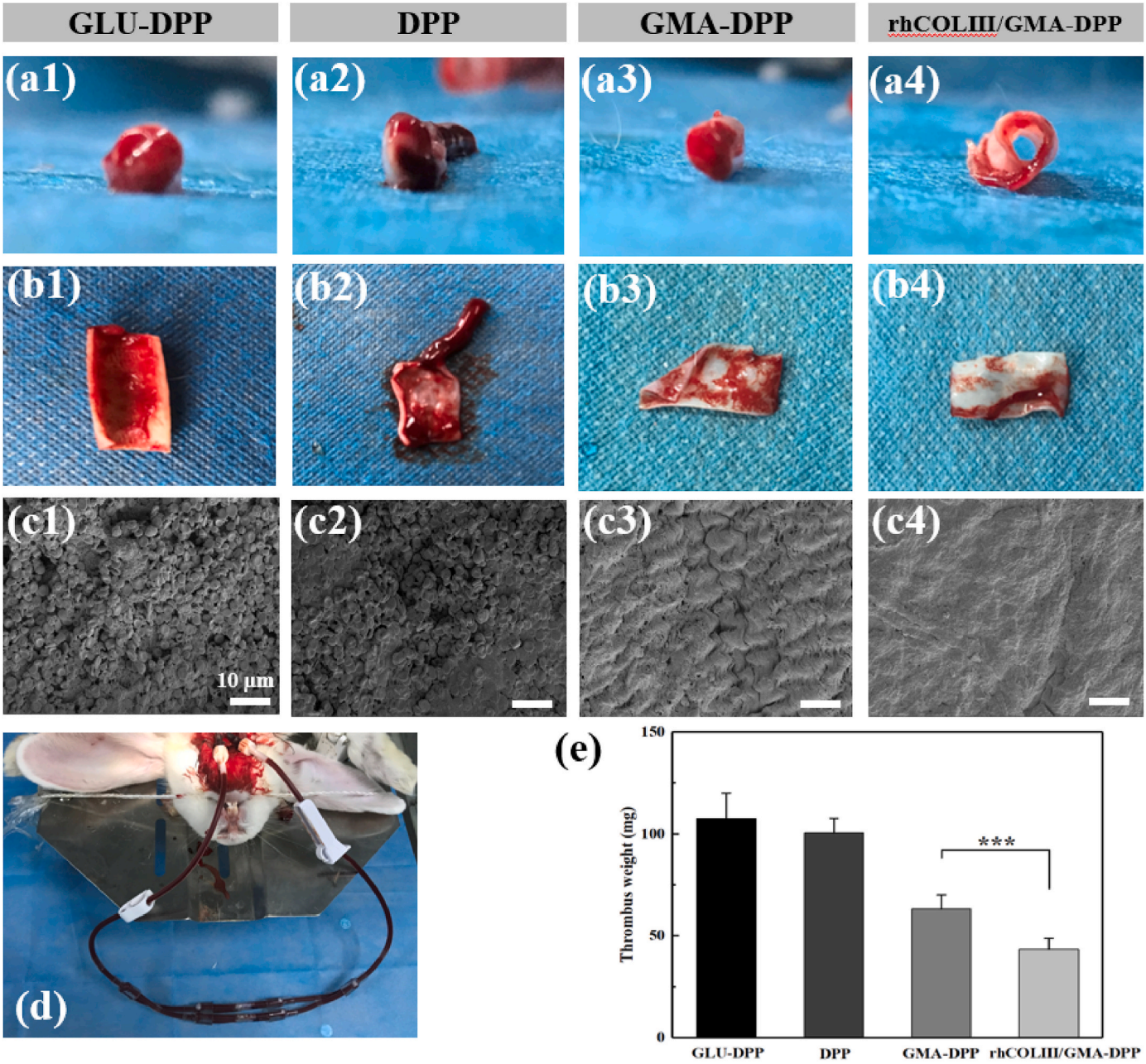

Fig. 7. Hemocompatibility. (a) Cross-section of tissues after 40 min of ex vivo blood circulation. (b) The surfaces of tissues after 40 min of in vitro blood circulation. (c) SEM images of tissues surfaces morphologies after in vitro blood circulation for 40 min. (d) Illustration of in vitro arteriovenous shunt assay. (e) Quantitative analysis of thrombus weight.

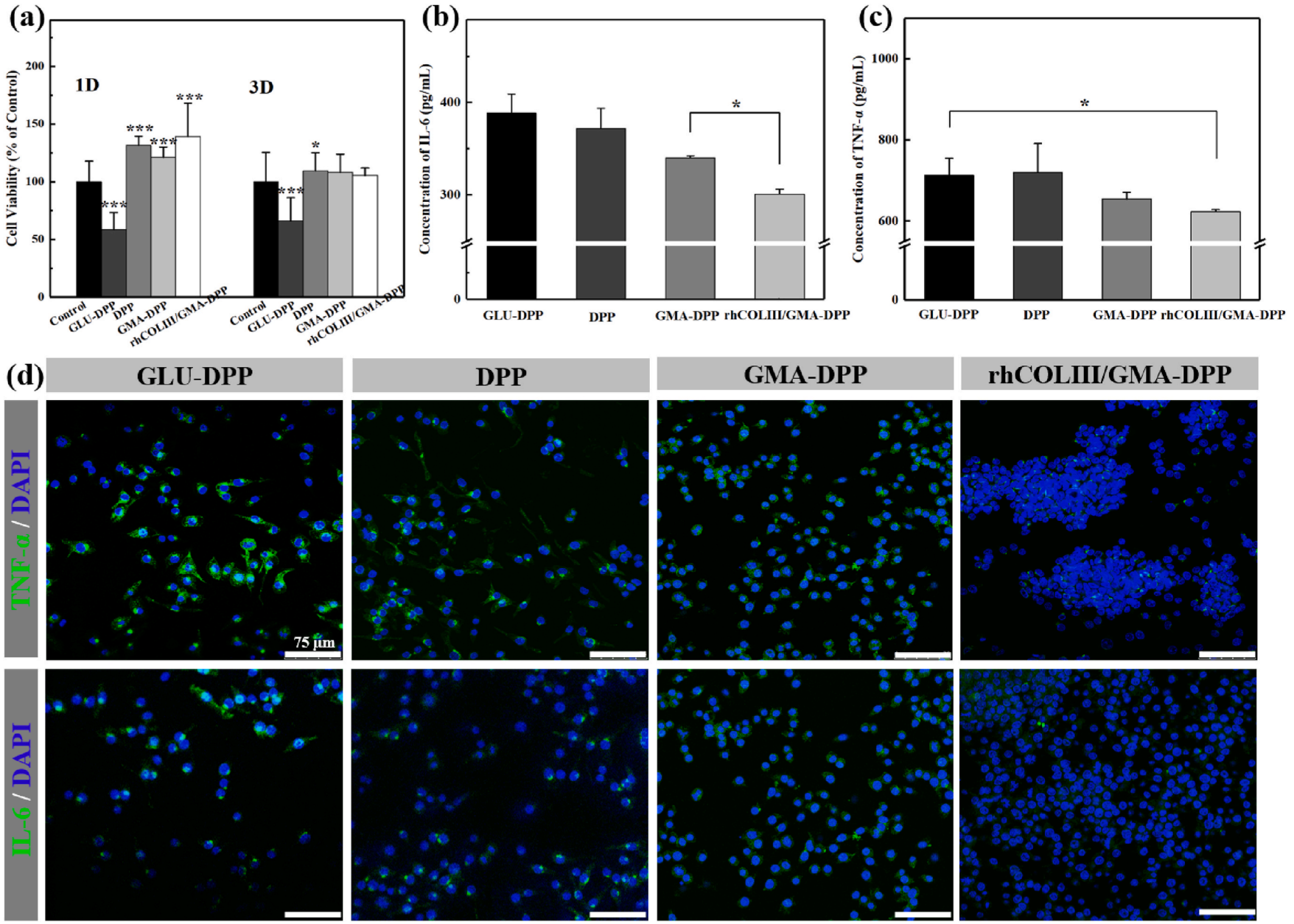

Fig. 8. (a) Cell viability of L929 after incubating with the extracts of GLU-DPP, DPP, GMA-DPP and rhCOLIII/GMA-DPP respectively for 1, 3 days. * represents the significant difference with the blank control. (b) IL-6 in the supernatant of Raw264.7 culture medium measured by ELISA Kits. (c) TNF-α in the supernatant of Raw264.7 culture medium measured by ELISA Kits. (d) Immunofluorescence staining of TNF-α and IL-6 for macrophages.

DPP, GMA-DPP and rhCOLIII/GMA-DPP and the absorbance of hemoglobin which reflected the amount of blood clot were displayed. Significantly, more red thrombi were observed on GLU-DPP and DPP than on GMA-DPP and rhCOLIII/GMA-DPP (Fig. 6a). To furthermore determine the amount of thrombi, the absorbance of hemoglobin was measured and the optical density (OD) value of rhCOLIII/GMA-DPP was the lowest (Fig. 6b).

To simulate real contact between materials and blood, an in vitro arteriovenous shunt test was performed to further evaluate antithrombogenic properties (Fig. 7d). According to Fig. 7a and b, the cross-section and surface images showed numerous thrombi were generated on GLU-DPP, DPP samples and blocked tubes. Compared with GMA-DPP, the thrombosis of rhCOLIII/GMA-DPP was significantly reduced and tubes were patent after 40 min of ex vivo blood circulation. As shown in Fig. 7e, the weight of thrombosis on rhCOLIII/GMA-DPP (43.4 ± 5.3 mg) was significantly reduced in contrast with that on GLU-DPP (107.5 ± 12.6 mg), DPP (100.5 ± 7.2 mg) and GMA-DPP (57.3 ± 6.9 mg). In accordance with the former results, merely a few platelets and erythrocytes attached to the surface of rhCOLIII/GMA-DPP, while substantial erythrocytes, activated platelets and fibrin networks were observed on GLU-DPP, DPP, GMA-DPP (Fig. 7c). These results suggested that the introduction of rhCOLIII could prominently improve the hemocompatibility of tissues.

3.6. Cytotoxicity

Cell viability of L929 cells after treating with extracts of GLU-DPP, DPP, GMA-DPP and rhCOLIII/GMA-DPP for 1, 3 days was presented in Fig. 8a. The cell viability was all higher than 90% in DPP, GMA-DPP and rhCOLIII/GMA-DPP groups, while it was lower than 65% in GLU-DPP group. The results demonstrated that rhCOLIII/GMA-DPP showed no cytotoxicity and performed well in cytocompatibility.

3.7. Immune response in vitro

Special chemokine was released by the activated macrophages to conduct other inflammatory cells and cytokines, finally leading to inflammation reaction. TNF-α acts as a proinflammatory role in inflammatory diseases and IL-6 is a potent pleiotropic cytokine, showing proinflammatory property. As demonstrated in Fig. 8b and c, the release of TNF-α and IL-6 were tested by ELISA Kits. The expression of IL-6 in rhCOLIII/GMA-DPP (300.8 ± 5.5 pg/ml) was significantly reduced in contrast with other groups. The expression of TNF-α in rhCOLIII/GMA-DPP (623.7 ± 4.2 pg/ml) was the lowest compared with other groups. As is shown in Fig. 8d, blue and green fluorescence represent macrophage nuclei and IL-6/TNF-α released by macrophages, respectively. In accord with quantitative data, the strongest green fluorescence is shown in GLU-DPP group, while the weakest in rhCOLIII/GMA-DPP group. All results indicating that rhCOLIII/GMA-DPP could reduce the inflammation response.

3.8. In vivo biocompatibility

To study the biocompatibility of tissues after the introduction of rhCOLIII in vivo, tissues were implanted subcutaneously in male SD rats for 7, 14, 28 days. In Fig. 9a, the images of H&E staining displayed obvious loose damaged tissues on DPP and GLU-DPP. In addition, the number of inflammatory cells around the tissue-scaffold interface were observed in GLU-DPP and DPP, while fewer on rhCOLIII/GMA-DPP and GMA-DPP. For immunohistochemical test, CD68 was applied to analyze immune response after implantations. As shown in Fig. 10a, a mass of CD68-marked macrophages gathered around the tissue-scaffold interface of DPP and GLU-DPP. But a small quantity of CD68-marked macrophages was recruited around the tissue-scaffold interface of rhCOLIII/GMA-DPP and GMA-DPP. Quantification of CD68-marked positive macrophages was shown in Fig. 10b and the results were consistent with images.

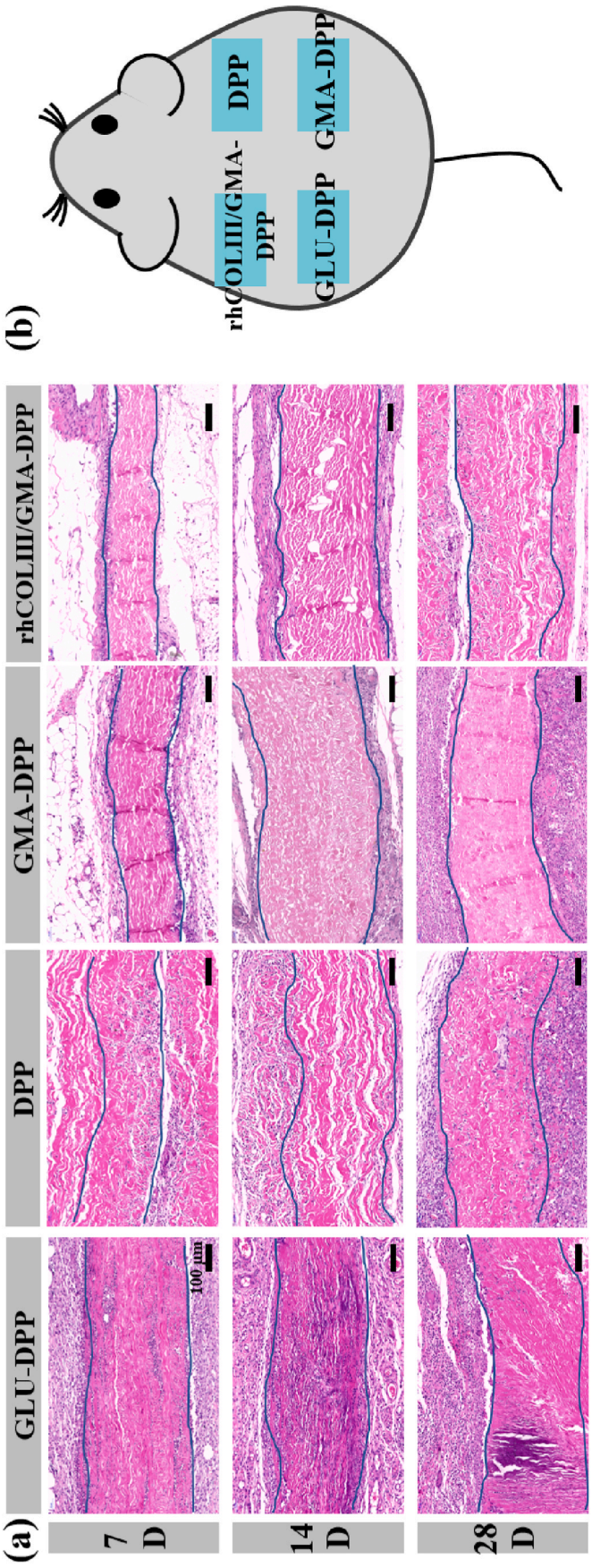

Fig. 9. In vivo biocompatibility. (a) HE staining of rhCOLIII/GMA-DPP, GMA-DPP, DPP and GLU-DPP at 7, 14 and 28 days after implantation in male SD rats. (b) Schematic diagram of subcutaneous implantation model.

Inflammatory factor IL-6 and TNF-α were selected to further study the inflammation response in vivo. As presented in Fig. 11a, the expression level of IL-6 and TNF-α was the highest for GLU-DPP, while the lowest in rhCOLIII/GMA-DPP. Quantification of IL-6 and TNF-α positives cells in Fig. 11b and c revealed the number of positive cells on rhCOLIII/GMA-DPP and GMA-DPP was significantly smaller than on DPP and GLU-DPP. And the expression of proinflammatory cytokines was the lowest in rhCOLIII/GMA-DPP group.

Calcification was the predominant mode of heart valve failure. An alizarin red staining assay and quantitative analysis were performed. According to Fig. 12a, the red spots represented calcification deposits. A few calcifications were deposited on rhCOLIII/GMA-DPP and GMA-DPP while severe calcification was observed on GLU-DPP and DPP. And the degree of calcification progressed as time went on. The calcium content of tissues was further quantitatively analyzed and it was the lowest in rhCOLIII/GMA-DPP. A series of biocompatibility tests in vivo confirmed that rhCOLIII/GMA-DPP possessed good biocompatibility with low expression of inflammatory factors and great anti-calcification properties.

4. Discussion

Large quantities of blood-contacting implantable devices have been widely used in many areas, such as heart valves, vascular grafts, artificial kidneys [37–40]. The biomaterials of these devices are required not to disadvantageously interact with any blood component, activate or destruct blood components [26,41]. AM is one of the most suitable biomaterials since it remains the structures, components and certain functions of extracellular matrix [42,43]. However, due to the exposure of highly thrombogenic collagen structures, residual cell debris and the genetic materials, and non-ideal crosslinking methods, some drawbacks still exist in AM, including non-ideal anticoagulation, negative inflammatory responses and poor mechanical properties, that may lead to reactions for patients, such as inflammation, fibrosis, coagulation, and infection. Hence, there is a pressing need for modified AM to reduce these risks [18,44,45].

The recent development of recombinant humanized collagen provides a possibility to solve these issues. In the complete amino acid sequence of human collagen type III, O-remaining fragments can readily bind to platelets' surface integrins α2β1, GP VI and GP Ib/IX/V complexes, thus activating platelets and inducing coagulation. Considering it, to acquire the recombinant humanized collagen with anticoagulation, rhCOLIII without O has been developed, which also remains cytocompatibility due to GER and GEK demonstrating stable triple-helix structure. Compared with traditional anticoagulants, it presents designability, low immunogenicity, good water solubility and no virus risk. In this study, a radical polymerization crosslinking DPP with rhCOLIII and GMA through one-pot method was prepared as artificial heart valves.

Before modification, decellularization is an essential prerequisite since the resident cell antigens and nucleic acid remnants may cause hyperacute/acute rejection, immune response in xenogeneic implanted tissues and calcification [46]. Triton X-100 as a non-ionic solution is generally applied in conjunction with sodium deoxycholate to obtain optimized decellularization results [15]. The outcomes of H&E, MT and analysis of DNA quantification test in NPP and DPP demonstrated that the decellularization was effective.

Collagen is regarded as the main component of heart valves. The collagen fibers constitute a dense network naturally and are primarily aligned following a circumferential direction, which endows heart valves possess load-bearing capacity to physiological stresses [47,48]. An essence of crosslinking AM is to crosslink collagen and form a protein network by the crosslinkers (bridge). The primary reason is to increase its resistance to enzymatic degradation [49]. In this study, GMA was selected to crosslink DPP and stabilize collagen. Epoxy group of GMA could react with free amino groups of DPP, and then methacrylate groups were introduced. Likewise, methacrylate groups were introduced

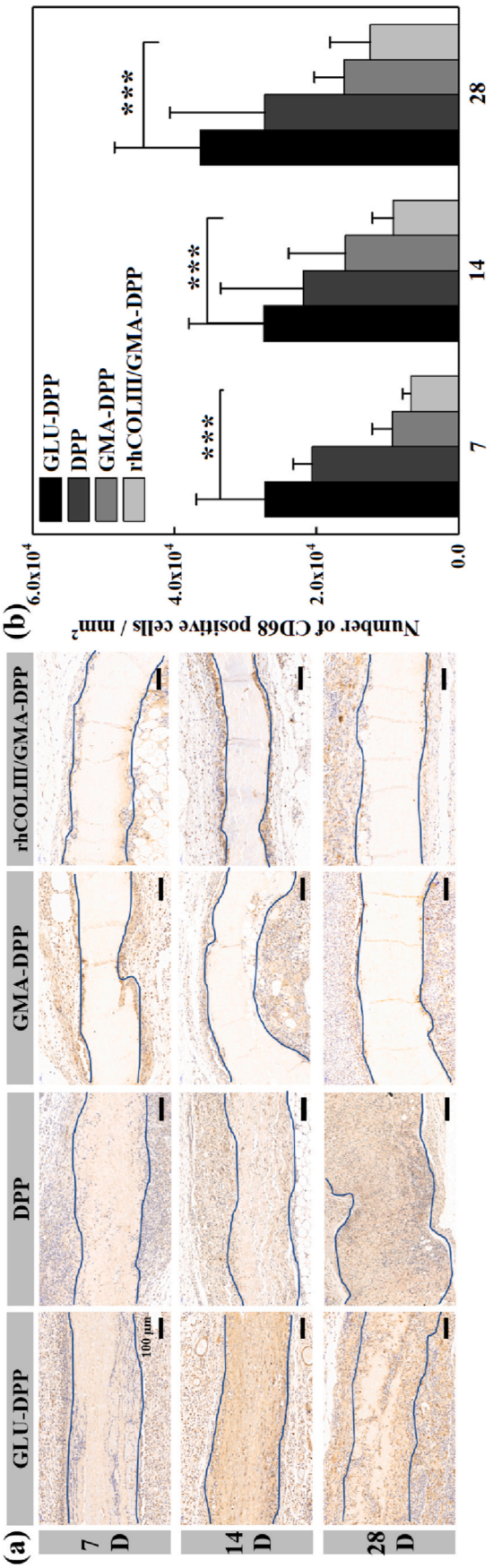

Fig. 10. In vivo biocompatibility. (a) Immunohistochemistry images of CD68 stained slices on rhCOLIII/GMA-DPP, GMA-DPP, DPP and GLU-DPP at 7, 14 and 28 days after implantation. (b) The numbers of CD68 positive cells surrounding implants were measured by a semi-quantitative analysis in accordance with immunohistochemistry slices.

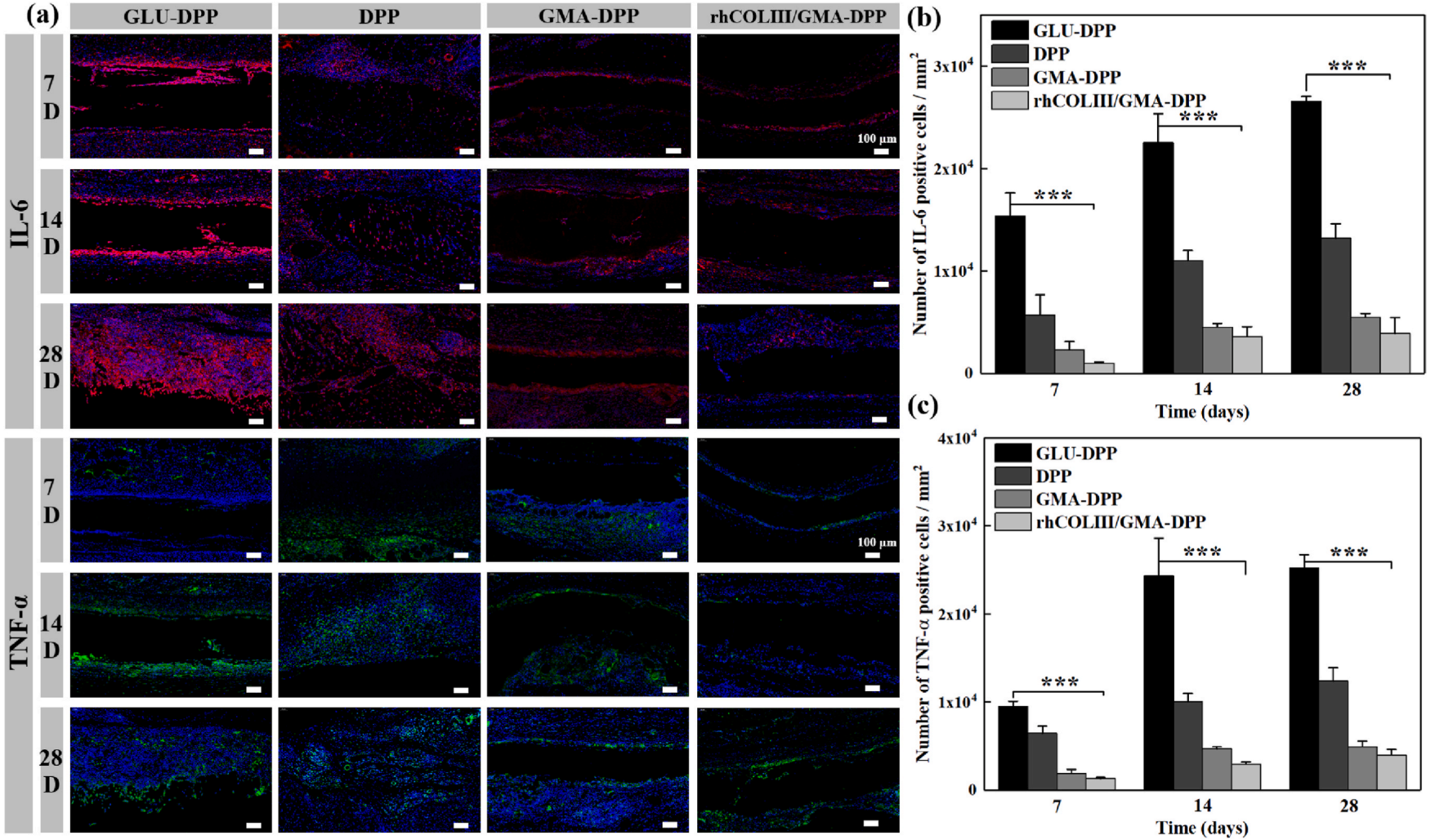

Fig. 11. In vivo biocompatibility. (a) Immunofluorescence images of IL-6 (red) and TNF-α (green) stained sections on rhCOLIII/GMA-DPP, GMA-DPP, DPP and GLU-DPP at 7, 14 and 28 days postimplantation. All scale bars are 100 μm. (b) The amount of IL-6 positive cells around the implants at 7, 14 and 28 days. (c) The amount of TNF-α positive cells around the implants at 7, 14 and 28 days. (For interpretation of the references to colour in this figure legend, the reader is referred to the Web version of this article.)

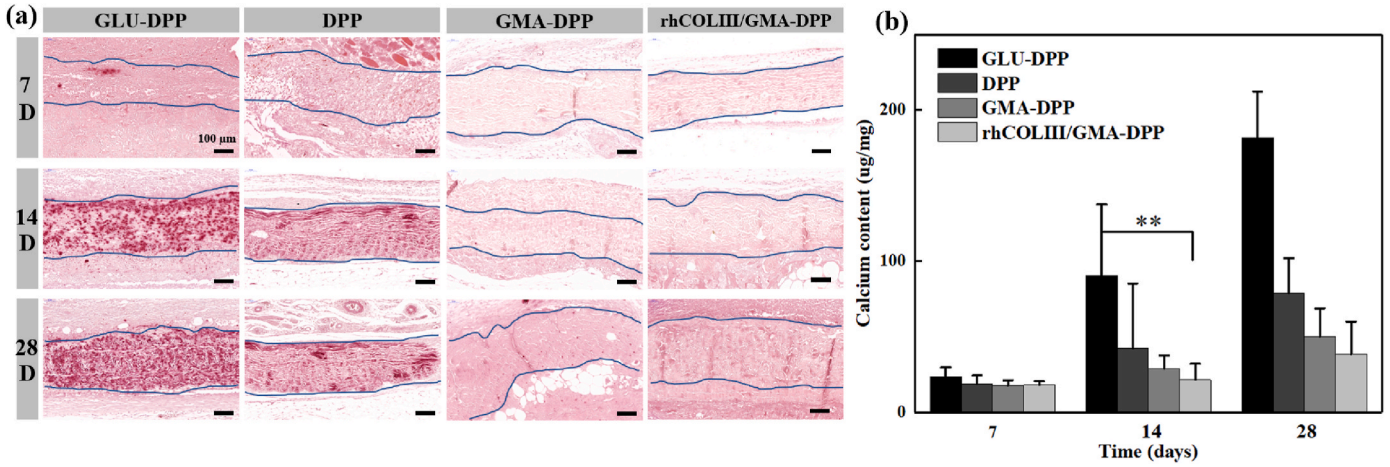

Fig. 12. In vivo biocompatibility. (a) Alizarin red staining of rhCOLIII/GMA-DPP, GMA-DPP, DPP and GLU-DPP at 7, 14 and 28 days after implantation in male SD rats. (b) Calcium contents of rhCOLIII/GMA-DPP, GMA-DPP, DPP and GLU-DPP at 7, 14 and 28 days were calculated. (For interpretation of the references to colour in this figure legend, the reader is referred to the Web version of this article.)

on rhCOLIII in the same way. The methacrylate groups could act as the bridge to crosslink DPP and introduce rhCOLIII on DPP by radical polymerization. The amino content of DPP and rhCOLIII before and after reaction changed significantly, confirming the successful introduction of methacrylate groups. Crosslinking degree can control the degradation rate of biological tissues. The results of enzymatic degradation experiment with different concentration of GMA proved that 5%GMA-DPP was optimal to stabilize collagen. To further characterize the physical and chemical structures, ATR-FTIR and 1H NMR were applied. The outcomes also confirmed the successful crosslinking of DPP, effective introduction of methacrylate groups on rhCOLIII, DPP and the introductions of rhCOLIII on DPP.

Mechanical properties to guide the development of the heart valve structure are indispensable for future design criteria [50]. The ability to offer adequate mechanical function instantly after implantation is vital for patients' survival [51]. Compared with DPP, the tensile strength of rhCOLIII/GMA-DPP significantly increased due to the formation of a crosslinking network. And the elongation of rhCOLIII/GMA-DPP was improved in contrast with GLU-DPP. Therefore, rhCOLIII/GMA-DPP possessed suitable mechanical properties.

Hemocompatibility is an important parameter to evaluate the introduction of rhCOLIII on crosslinked DPP. Platelets interacting with the surface of rhCOLIII/GMA-DPP is crucial for forming thrombus [52]. And the deposition of aggregated platelets on the surface is stabilized by fibrin strands, forming a platelet-fibrin thrombus [53]. Thrombin and kallikrein activate complement, thereby resulting in local inflammatory responses. In this study, platelets adhered to rhCOLIII/GMA-DPP were markedly the least, compared with GLU-DPP, DPP and GMA-DPP. The reason may be related to the introduction of rhCOLIII which was designed without the sequences containing O which readily bound to platelet surface integrins. Likewise, the results of recalcification whole blood clotting assay and in vitro arteriovenous shunt test confirmed good blood capability in rhCOLIII/GMA-DPP as well. The reason for poor blood compatibility of DPP is that the exposure of a highly thrombogenic collagen surface after decellularization will induce to adhere and activate platelets and release coagulation factor XII [54]. For GLU-DPP, the reason for poor blood compatibility may be related to the decreased water content of heart valves, contracted protein structure due to strong crosslinking effect and rough surface structure after treatment of glu [55].

Cytocompatibility is one of the vital parameters of biomaterials for application in heart valves [56]. According to the results, the cell viability of DPP, GMA-DPP and rhCOLIII/GMA-DPP groups was all higher than 90%, while GLU-DPP group was lower than 65%. The results demonstrating that rhCOLIII/GMA-DPP showed no cytotoxicity and performed well in cytocompatibility. The toxicity of glu crosslinker would impede the endothelialization of heart valves.

In vivo biocompatibility was further characterized upon subcutaneous implantation in SD male rats for 7, 14, 28 days. After implantation, the body will be protected from foreign implants by immune response and inflammatory cells will be recruited around the tissue-scaffold interface, which is considered to related to the immune response [57,58]. The images of H&E staining illustrating inflammatory cells around the tissue-scaffold interface and damaged tissues were found in DPP and GLU-DPP. The results of CD68-marked macrophages also verified that GLU-DPP and DPP induced more severe inflammatory response than rhCOLIII/GMA-DPP and GMA-DPP after implantation. The glu fixing may reduce immune response but it could not eliminate the immune response to allografts and xenografts completely. Similarly, despite decellularization, the cell debris and the genetic materials could not be removed completely. Therefore, DPP could induce immune response as well. rhCOLIII was originated from bioactive peptide sequences of human type III collagen, which possesses designability, low immunogenicity, good water solubility and no virus risk. The introduction of rhCOLIII on crosslinked DPP helped to decrease the immune response. To further study the inflammation response in vivo, inflammatory factor IL-6 and TNF-α were selected. IL-6 is a pleiotropic cytokine and shows proinflammatory properties after inflammatory stimulation. TNF-α presents both immunoregulatory and proinflammatory properties of cytokines [59]. Expression of IL-6 and TNF-α was the lowest in rhCOLIII/GMA-DPP and the highest in GLU-DPP. The results of H&E staining, CD68-marked macrophages assay and inflammatory factor characterization all confirming the slightest inflammatory response of rhCOLIII/GMA-DPP. Calcification is one of the vital factors to affect the long-term safety and performance of heart valves. The mechanism of calcification is complex and not thoroughly comprehended, which concludes degradation of extracellular matrix, crosslinking chemistry, and immune response. In this study, the calcification of GLU-DPP and DPP was severe after implantation for 14 and 21 days. For GLU-DPP, the use of glu to minimize antigenicity comes at the expense of the introduction of a residual aldehyde group on heart valves, which possesses high Ca^{2+} affinity [60,61]. In this study, the reduction of inflammatory response and no residual aldehyde groups may contribute to anti-calcification of rhCOLIII/GMA-DPP.

5. Conclusion

In this paper, we introduced a simple strategy of functional

crosslinking AM in application of blood-contacting implantable devices. A radical-polymerization-crosslinked DPP with anticoagulation properties through one-pot method was designed as artificial heart valves. GMA acted as the crosslinker and rhCOLIII without platelet binding sites, provided anticoagulation properties. Compared with other crosslinking strategies, we used one-pot method to crosslink AM and introduce biological activities simultaneously. In addition, gentle reaction conditions and diversified monomers of free radical polymerization were beneficial to the chemical reaction of biological matrices. This study is aiming to offer a simple strategy for functionalizing cross-linked AM and possibilities for real application when applying in blood-contacting implantable devices.

Author statement

Yao Ge: Conceptualization, Methodology, Formal analysis, Investigation, Data Curation, Writing-Original Draft. **Gaoyang Guo:** Validation, Formal analysis, Visualization, Software. **Kunpeng Liu:** Formal analysis, Resources. **Fan Yang:** Resources. **Li Yang:** Resources, Writing-review & editing, Funding acquisition. **Yunbing Wang:** Resources, Writing-review & editing, Funding acquisition. **Xingdong Zhang:** Resources.

Declaration of competing interest

The authors declare that they have no known competing financial interests or personal relationships that could have appeared to influence the work reported in this paper.

Acknowledgements

This research was supported by National Key Research and Development Programs, China (2020YFC1107802), National Natural Science Foundation of China (32101107, 32071357), the 111 Project of Introducing Talents of Discipline to Universities, China (No. B16033), and the Fundamental Research Funds for the Central Universities, China (YJ201641). Thank Venus Medical Appliances Co., Ltd. (Hangzhou, China) for offering us fresh pericardium, Jingbo Co., Ltd. (Shanxi, China) for offering us rhCOLIII.

References

[1] Crapo PM, Gilbert TW, Badylak SF. An overview of tissue and whole organ decellularization processes. Biomaterials 2011;32(12):3233–43.
[2] Wu C, Pan J, Bao Z, Yu Y. Fabrication and characterization of chitosan microcarrier for hepatocyte culture. J Mater Sci Mater Med 2007;18(11):2211–4.
[3] Van Sweringen HL, Sakai N, Quillin RC, Bailey J, Schuster R, Blanchard J, et al. Roles of hepatocyte and myeloid CXC chemokine receptor-2 in liver recovery and regeneration after ischemia/reperfusion in mice. Hepatology 2013;57(1):331–8.
[4] Seglen PO. Chapter 4 preparation of isolated rat liver cells. 1976. p. 29–83.
[5] Li Y, Wang J, Wang Y, Cui W. Advanced electrospun hydrogel fibers for wound healing. Compos B Eng 2021:223.
[6] Meyer SR, Nagendran J, Desai LS, Rayat GR, Churchill TA, Anderson CC, et al. Decellularization reduces the immune response to aortic valve allografts in the rat. J Thorac Cardiovasc Surg 2005;130(2):469–76.
[7] Zhou J, Fritze O, Schleicher M, Wendel HP, Schenke-Layland K, Harasztosi C, et al. Impact of heart valve decellularization on 3-D ultrastructure, immunogenicity and thrombogenicity. Biomaterials 2010;31(9):2549–54.
[8] Schenke-Layland K, Vasilevski O, Opitz F, Konig K, Riemann I, Halbhuber KJ, et al. Impact of decellularization of xenogeneic tissue on extracellular matrix integrity for tissue engineering of heart valves. J Struct Biol 2003;143(3):201–8.
[9] Gbyli R, Mercaldi A, Sundaram H, Amoako KA. Achieving totally local anticoagulation on blood contacting devices. Adv Mater Interfac 2018;5(4).
[10] Frost MC, Reynolds MM, Meyerhoff ME. Polymers incorporating nitric oxide releasing/generating substances for improved biocompatibility of blood-contacting medical devices. Biomaterials 2005;26(14):1685–93.
[11] Radke D, Jia W, Sharma D, Fena K, Wang G, Goldman J, et al. Tissue engineering at the blood-contacting surface: a review of challenges and strategies in vascular graft development. Adv. Health. Mater. 2018;7(15):e1701461.
[12] Wang H-J, Mao Q-Y, Feng G, Liu C, Yang M-Z, Hao M-F, et al. 3D printing of multifunctional artificial conduits against acute thrombosis and clinical infection. Compos B Eng 2022:230.
[13] Sefton MV, Gemmell CH, Gorbet MB. What really is blood compatibility? J Biomater Sci Polym Ed 2000;11(11):1165–82.
[14] Labarrere CA, Dabiri AE, Kassab GS. Thrombogenic and inflammatory reactions to biomaterials in medical devices. Front Bioeng Biotechnol 2020;8:123.
[15] Dettin M, Zamuner A, Naso F, Monteleone A, Spina M, Gerosa G. Natural scaffolds for regenerative medicine: direct determination of detergents entrapped in decellularized heart valves. 2017 BioMed Res Int 2017:9274135.
[16] Yu Y, Zhang W, Liu X, Wang H, Shen J, Xiao H, et al. Extracellular matrix scaffold-immune microenvironment modulates tissue regeneration. Compos B Eng 2022:230.
[17] Soletti L, Nieponice A, Guan J, Stankus JJ, Wagner WR, Vorp DA. A seeding device for tissue engineered tubular structures. Biomaterials 2006;27(28):4863–70.
[18] Liu C, Qiao W, Cao H, Dai J, Li F, Shi J, et al. A riboflavin-ultraviolet light A-crosslinked decellularized heart valve for improved biomechanical properties, stability, and biocompatibility. Biomater. Sci. 2020;8(9):2549–63.
[19] de Mel A, Cousins BG, Seifalian AM. Surface modification of biomaterials: a quest for blood compatibility. 2012 Int J Biomater 2012:707863.
[20] Maitz MF, Martins MCL, Grabow N, Matschegewski C, Huang N, Chaikof EL, et al. The blood compatibility challenge. Part 4: surface modification for hemocompatible materials: passive and active approaches to guide blood-material interactions. Acta Biomater 2019;94:33–43.
[21] Dai J, Qiao W, Shi J, Liu C, Hu X, Dong N. Modifying decellularized aortic valve scaffolds with stromal cell-derived factor-1alpha loaded proteolytically degradable hydrogel for recellularization and remodeling. Acta Biomater 2019;88:280–92.
[22] Brash JL, Horbett TA, Latour RA, Tengvall P. The blood compatibility challenge. Part 2: protein adsorption phenomena governing blood reactivity. Acta Biomater 2019;94:11–24.
[23] Ma L, Cheng C, Nie C, He C, Deng J, Wang L, et al. Anticoagulant sodium alginate sulfates and their mussel-inspired heparin-mimetic coatings. J Mater Chem B 2016;4(19):3203–15.
[24] Koh CY, Kini RM. Molecular diversity of anticoagulants from haematophagous animals. Thromb Haemostasis 2009;102(3):437–53.
[25] Sotiri I, Robichaud M, Lee D, Braune S, Gorbet M, Ratner BD, et al. BloodSurf 2017: news from the blood-biomaterial frontier. Acta Biomater 2019;87:55–60.
[26] Weber M, Steinle H, Golombek S, Hann L, Schlensak C, Wendel HP, et al. Blood-contacting biomaterials: in vitro evaluation of the hemocompatibility. Front Bioeng Biotechnol 2018;6:99.
[27] Wong ML, Griffiths LG. Immunogenicity in xenogeneic scaffold generation: antigen removal vs. decellularization. Acta Biomater 2014;10(5):1806–16.
[28] Liu W, Merrett K, Griffith M, Fagerholm P, Dravida S, Heyne B, et al. Recombinant human collagen for tissue engineered corneal substitutes. Biomaterials 2008;29(9):1147–58.
[29] Wang T, Lew J, Premkumar J, Poh CL, Win Naing M. Production of recombinant collagen: state of the art and challenges. Eng. Biol. 2017;1(1):18–23.
[30] Perret S, Eble JA, Siljander PR, Merle C, Farndale RW, Theisen M, et al. Prolyl hydroxylation of collagen type I is required for efficient binding to integrin alpha 1 beta 1 and platelet glycoprotein VI but not to alpha 2 beta 1. J Biol Chem 2003;278(32):29873–9.
[31] Yang L, Wu H, Lu L, He Q, Xi B, Yu H, et al. A tailored extracellular matrix (ECM) - mimetic coating for cardiovascular stents by stepwise assembly of hyaluronic acid and recombinant human type III collagen. Biomaterials 2021;276:121055.
[32] Hua C, Zhu Y, Xu W, Ye S, Zhang R, Lu L, et al. Characterization by high-resolution crystal structure analysis of a triple-helix region of human collagen type III with potent cell adhesion activity. Biochem Biophys Res Commun 2019;508(4):1018–23.
[33] Guo G, Jin L, Jin W, Chen L, Lei Y, Wang Y. Radical polymerization-crosslinking method for improving extracellular matrix stability in bioprosthetic heart valves with reduced potential for calcification and inflammatory response. Acta Biomater 2018;82:44–55.
[34] Jin L, Guo G, Jin W, Lei Y, Wang Y. Cross-linking methacrylated porcine pericardium by radical polymerization confers enhanced extracellular matrix stability, reduced calcification, and mitigated immune response to bioprosthetic heart valves. ACS Biomater Sci Eng 2019;5(4):1822–32.
[35] Hayashi Y. Pot economy and one-pot synthesis. Chem Sci 2016;7(2):866–80.
[36] Zhao N, Yuan W. Highly adhesive and dual-crosslinking hydrogel via one-pot self-initiated polymerization for efficient antibacterial, antifouling and full-thickness wound healing. Compos B Eng 2022:230.
[37] Gong YY, Xue JX, Zhang WJ, Zhou GD, Liu W, Cao Y. A sandwich model for engineering cartilage with acellular cartilage sheets and chondrocytes. Biomaterials 2011;32(9):2265–73.
[38] Gamba PG, Conconi MT, Lo Piccolo R, Zara G, Spinazzi R, Parnigotto PP. Experimental abdominal wall defect repaired with acellular matrix. Pediatr Surg Int 2002;18(5–6):327–31.
[39] Mantovani F, Trinchieri A, Castelnuovo C, Romanò AL, Pisani E. Reconstructive urethroplasty using porcine acellular matrix. Eur Urol 2003;44(5):600–2.
[40] Li J, Wang S, Sheng Y, Liu C, Xue Z, Tong P, et al. Designing HA/PEI nanoparticle composite coating on biodegradable Mg–Zn–Y-Nd alloy to direct cardiovascular cells fate. Smart Mater. Med. 2021;2:124–33.
[41] Zheng C, Ding K, Huang X, Li M, Wu B, Lei Y, et al. Nonglutaraldehyde crosslinked bioprosthetic heart valves based on 2-isocyanatoethyl methacrylate crosslinked porcine pericardium with improved properties of stability, cytocompatibility and anti-calcification. Compos B Eng 2022:230.
[42] Wang Y, Cui CB, Yamauchi M, Miguez P, Roach M, Malavarca R, et al. Lineage restriction of human hepatic stem cells to mature fates is made efficient by tissue-specific biomatrix scaffolds. Hepatology 2011;53(1):293–305.

[43] Takashi H, Katsumi M, Toshihiro A. Hepatocytes maintain their function on basement membrane formed by epithelial cells. Biochem Biophys Res Commun 2007;359(1):151–6.
[44] Liang HC, Chang Y, Hsu CK, Lee MH, Sung HW. Effects of crosslinking degree of an acellular biological tissue on its tissue regeneration pattern. Biomaterials 2004;25 (17):3541–52.
[45] Baddour JA, Sousounis K, Tsonis PA. Organ repair and regeneration: an overview. Birth Defects Res C Embryo Today 2012;96(1):1–29.
[46] Naso F, Gandaglia A. Different approaches to heart valve decellularization: a comprehensive overview of the past 30 years. Xenotransplantation 2018;25(1).
[47] Kramer KE, Ross CJ, Laurence DW, Babu AR, Wu Y, Towner RA, et al. An investigation of layer-specific tissue biomechanics of porcine atrioventricular valve anterior leaflets. Acta Biomater 2019;96:368–84.
[48] Eriksen HA, Satta J, Risteli J, Veijola M, Vare P, Soini Y. Type I and type III collagen synthesis and composition in the valve matrix in aortic valve stenosis. Atherosclerosis 2006;189(1):91–8.
[49] Elder S, Pinheiro A, Young C, Smith P, Wright E. Evaluation of genipin for stabilization of decellularized porcine cartilage. J Orthop Res 2017;35(9):1949–57.
[50] Dijkman PE, Driessen-Mol A, Frese L, Hoerstrup SP, Baaijens FP. Decellularized homologous tissue-engineered heart valves as off-the-shelf alternatives to xeno- and homografts. Biomaterials 2012;33(18):4545–54.
[51] Hasan A, Ragaert K, Swieszkowski W, Selimovic S, Paul A, Camci-Unal G, et al. Biomechanical properties of native and tissue engineered heart valve constructs. J Biomech 2014;47(9):1949–63.
[52] Makris M, Calizzani G, Fischer K, Gilman EA, Hay CRM, Lassila R, et al. EUHASS: the European haemophilia safety surveillance system. Thromb Res 2011;127: S22–5.
[53] Li JA, Chen L, Zhang XQ, Guan SK. Enhancing biocompatibility and corrosion resistance of biodegradable Mg-Zn-Y-Nd alloy by preparing PDA/HA coating for potential application of cardiovascular biomaterials. Mater Sci Eng C Mater Biol Appl 2020;109:110607.
[54] Stamm C, Khosravi A, Grabow N, Schmohl K, Treckmann N, Drechsel A, et al. Biomatrix/polymer composite material for heart valve tissue engineering. Ann Thorac Surg 2004;78(6):2084–92. discussion 92-93.
[55] Yang F, Xu L, Kuang D, Ge Y, Guo G, Wang Y. Polyzwitterion-crosslinked hybrid tissue with antithrombogenicity, endothelialization, anticalcification properties. Chem Eng J 2021:410.
[56] Barros JA, Filippin-Monteiro FB, de Oliveira EM, Campa A, Catalani LH, Pitombo Rde N, et al. Cytotoxicity of PVPAC-treated bovine pericardium: a potential replacement for glutaraldehyde in biological heart valves. J Biomed Mater Res B Appl Biomater 2014;102(3):574–82.
[57] Zilla P, Brink J, Human P, Bezuidenhout D. Prosthetic heart valves: catering for the few. Biomaterials 2008;29(4):385–406.
[58] Heath DE. Promoting endothelialization of polymeric cardiovascular biomaterials. Macromol Chem Phys 2017;218(8).
[59] Umare V, Pradhan V, Nadkar M, Rajadhyaksha A, Patwardhan M, Ghosh KK, et al. Effect of proinflammatory cytokines (IL-6, TNF-alpha, and IL-1beta) on clinical manifestations in Indian SLE patients. 2014 Mediat Inflamm 2014:385297.
[60] Hartgerink JD, Beniash E, Stupp SI. Self-assembly and mineralization of peptide-amphiphile nanofibers. Science 2001;294(5547):1684–8.
[61] Kato R, Nakamura S, Katayama K, Yamashita K. Electrical polarization of plasma-spray-hydroxyapatite coatings for improvement of osteoconduction of implants. J Biomed Mater Res 2005;74(4):652–8.